Techno-economic analysis of energy storage systems integrated with ultra-fast charging stations

A dutch case study

Ahmad, A.; Meyboom, J.; Bauer, P.; Qin, Z.

DOI
10.1016/j.etran.2025.100411

Publication date
2025

Document Version
Final published version

Published in
eTransportation

eTransportation 24 (2025) 100411

Contents lists available at ScienceDirect

eTransportation

journal homepage: www.journals.elsevier.com/etransportation

Techno-economic analysis of energy storage systems integrated with ultra-fast charging stations: A dutch case study

A. Ahmad, J. Meyboom, P. Bauer, Z. Qin *

Department of Electrical Sustainable Energy, Delft University of Technology, Delft 2628 CD, The Netherlands

ARTICLE INFO

Keywords:
Electric vehicles
Ultra-fast charging stations
Battery energy storage systems
Dynamic pricing
Operational expenses

ABSTRACT

A fast and efficient charging infrastructure has become indispensable in the evolving energy landscape and thriving electric vehicle (EV) market. Irrespective of the charging stations' internal alternating current (AC) or direct current (DC) bus configurations, the main concern is the exponential growth in charging demands, resulting in network congestion issues. In the context of exponential EV growth and the provision of charging facilities from low-voltage distribution networks, the distribution network may require frequent upgrades to meet the rising charging demands. To avoid network congestion problems and minimize operational expenses (OE) by integrating energy storage systems (ESS) into ultra-fast charging stations (UFCS). This paper presents a techno-economic analysis of a UFCS equipped with a battery ESS (BESS). To reduce reliance on the electric grid and minimize OE, a dual-objective optimization problem is formulated and solved via grid search and dual-simplex algorithms. Analytical energy and physical BESS models are employed to evaluate the optimization matrices. The intricacies of BESS aging are examined to ensure an optimal BESS size with a more extensive lifespan than the corresponding payback period. The integrated BESS significantly reduced reliance on the grid to tackle network congestion while fulfilling charging demands. The dynamic pricing (DP) structure has proven more favorable, as the average per unit cost remains lower than the static tariff (ST). Results illustrate that integrating BESS reduces the OE and peak-to-average ratio (PAR) by 5-to-49% and 16-to-73%, respectively. Moreover, the combination of 70% BESS and 30% grid capacities outperforms the other configurations with a 73% reduction in PAR and a 49% reduction in OE before BESS reaches the end-of-life.

1. Introduction

Electric vehicles (EVs) have faced three significant challenges: high price, range anxiety, and lack of charging infrastructure. A combination of subsidies and technological breakthroughs neutralized the first two constraints significantly. However, the fundamental issue of charging infrastructure related to network capacity and congestion must be addressed to facilitate a smooth transition. Unlike conventional gasoline refilling stations with local storage tanks, the alternative charging infrastructure poses unique attributes and challenges due to its online connection with the electric grid. The power system represents one of the most complex and expansive engineered systems ever developed and maintained by humans. However, its history also has fatal blackouts, such as the Odessa disturbance [1]. Therefore, any unplanned and uncontrolled charging activity in ultra-fast charging stations (UFCS) can create a severe demand–supply imbalance and trigger a catastrophic failure.

Moreover, the European Union's (EU) commitment to the Paris agreement, exponential growth in EVs and the corresponding charging demands put significant stress on the Continental synchronous area grid and the Dutch energy grid [2]. Although the rise in EVs is impressive, it has drawbacks, such as grid congestion, and the magnitude of the Netherlands's grid congestion problem is already staggering. Moreover, it seems challenging to fulfill the immense power demands of the Netherlands' growing electric mobility (e-mobility) sector from the nearly overloaded distribution network, as shown in Fig. 1 [3]. Although, the present Dutch low-voltage (LV) distribution network is very well-designed to empower residential and small-scale commercial consumers. However, providing charging facilities to EVs can lead towards overloading and tripping scenarios. Fig. 1 resembles the situation indicated by the California public utilities commission's research that the distribution network will need significant upgrades as the charging infrastructure expands over the generation and transmission sectors [4].

In 2024, the number of on-road EVs will reach around 17 million, indicating the worldwide trend towards e-mobility and emphasizing

* Corresponding author.
E-mail addresses: A.Ahmad-2@tudelft.nl (A. Ahmad), jaspermeyboom@gmail.com, J.O.Meyboom@student.tudelft.nl (J. Meyboom), P.Bauer@tudelft.nl (P. Bauer), Z.Qin-2@tudelft.nl (Z. Qin).

https://doi.org/10.1016/j.etran.2025.100411
Received 18 July 2024; Received in revised form 20 February 2025; Accepted 26 February 2025
Available online 12 March 2025

Nomenclature

A	Exponential voltage (V)	Γ	Cell-to-ambient thermal time constant (s)
B	Exponential capacity (Ah^{-1})	κ	Real number ($\kappa = 1.....\infty$)
C	Nominal discharge curve slope (VA^{-1} h^{-1})	$\mathcal{L}$	Laplace transformation
c	Extracted capacity (Ah)	ψ	Arrhenius rate constant for the cycle number
DD	Cycle depth (–)	σ	(dis)charging status ((0)1)
E	Energy stored(released) (Wh)	τ	Time slot (10-min)
e	Exponential factor (–)	ϱ	Thermal resistance (°C/W)
f	Complex function (–)	ξ	DD exponential factor
h	Half cycle duration (s)	ϱ	Thermal resistance (°C/W)
H	Cycle number constant (–)	ζ	Number of (dis)charging slots
$\overline{I}$	Average current (A)	Subscripts	
i	Current (A)	a	Ambient
j	Number of chargers (–)	b	Battery
K	Polarization constants (VA^{-1} h^{-1})	bmin	Battery minimum
k	(dis)charging status ((−1)1)	bmax	Battery maximum
N	Maximum number of cycles (–)	bol	Beginning-of-life
n	Dynamic number of cycles (–)	c	Charger
P	Power (W)	ch	Charge
Q	Maximum capacity (Ah)	d	Demand
R	Resistance (Ω)	dis	Discharge
T	Temperature (°K)	ev	Electric vehicle
t	Time (s)	eol	End-of-life
V	Voltage (V)	g	Grid
Greek symbols		gmin	Grid minimum
α	Arrhenius rate constants of polarization resistance (–)	gmax	Grid maximum
β	Arrhenius rate constants internal resistance (–)	l	Low frequency dynamics
η	Conversion efficiency (%)	Ref	Nominal
ϵ	Aging factor (–)	tl	Thermal loss
γ	Current exponential factor (–)	0	Constant

the need for fast and efficient charging infrastructure [5]. The power system must have sufficient capacity to ensure a seamless transition, but direct access to strong electric grids is only possible in some regions. At the same time, a UFCS with EV chargers of ≥100 kW requires a substantial amount of power to meet the charging demands. Although innovative charging techniques have been investigated for EVs, they are best suited for overnight home charging, not for fast charging at the UFCS. In order to facilitate the development of alternative charging infrastructure, significant upfront investments are required for grid reinforcement. On the other hand, a UFCS network with a dedicated medium voltage (MV) grid connection and inherent storage feature can replicate gasoline infrastructure. It can mitigate the grid reinforcement and allow the charging of EVs at higher power levels due to the integrated battery energy storage system (BESS) [6]. Additionally, deploying a BESS is less expensive and complicated than grid reinforcement.

Although the charging infrastructure has a significant peak power demand, the probability of simultaneous charging due to multiple charging slots in UFCSs is less and average demand remains minimal. The real-time data and load profile of one of the fastest-growing charging networks in the Netherlands, i.e., FastNed network, also indicate that average consumption remains much lower [7,8]. Interestingly, the solution lies within the analysis of the load curves and utilization factors of the charging slots available in the UFCS. As mentioned earlier, the solution involves integrating BESS into UFCSs that mimic the inherent storage feature of gasoline stations. The BESS leverages the lower average power need and alleviates peak power demand. However, the induction of BESS comes with financial burdens on UFCS owners, and proper techno-economic analysis is required to select the optimal BESS size with a significant lifespan and small payback period.

This paper investigates the two interconnected aspects of BESS, i.e., sizing and integration for practical, sustainable, and economically viable e-mobility solutions. Sizing involves the optimal BESS and grid connection sizes to reduce the reliance on the grid. It mitigates the grid congestion issue and ensures an uninterrupted power supply for EV charging. Integration refers to scheduling the BESS's (dis)charge

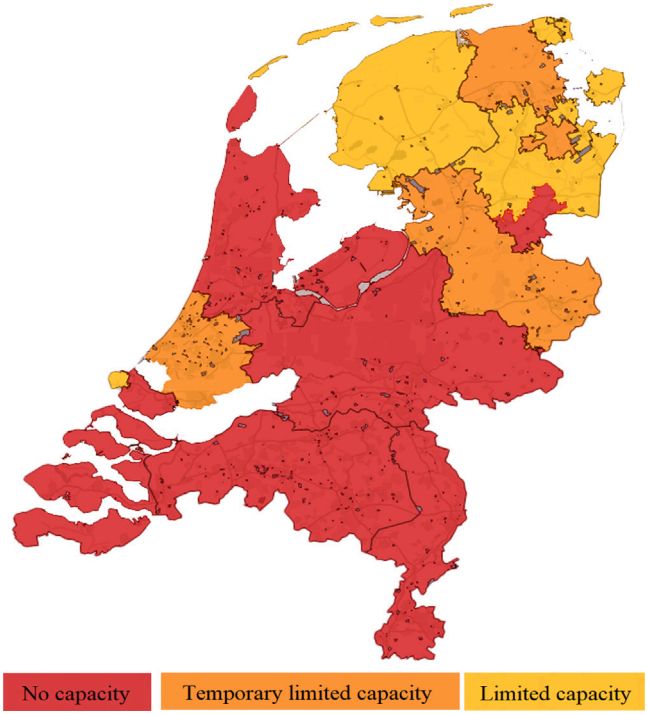

Fig. 1. The Netherlands's network status to accommodate new loads [3].

processes based on demand profile and electricity prices. Moreover, charging a BESS in off-peak and/or low-price slots and discharging it in peak and/or high-price slots reduces the UFCS's operational expenditures (OE) and ensures a reduced peak-to-average ratio (PAR). From the utility perspective, PAR is crucial to flatten the load profile and reduce the need for spinning reserves. The PAR is interconnected with the OE, as a higher PAR results in high OE and vice versa. The peak demand charges due to a high PAR are defined in [9] as "a demand charge is a fee based on the highest rate, measured in kW, at which electricity is drawn during any 15-to-30-min interval in the monthly billing period".

We aimed at the modeling of a BESS-integrated UFCS consisting of 50-to-350 kW chargers with a cumulative charging demand of 3.5 MW. Our primary objective is to reduce dependency on the electric grid and fulfill the 3.5 MW power demand of nineteen fast and ultrafast chargers, i.e., six 350 kW, six 175 kW and seven 50 kW chargers with a 1 MW grid connection, by introducing a 2.5 MWh storage feature to the UFCS. The proposed model efficiently utilizes limited energy resources to address the network congestion issue. The second objective in this dual-optimization problem is to minimize the OE, a combination of demand tariffs and actual energy consumption (EC) costs, further explained in Section 3.

To thoroughly examine this critical yet frequently overlooked aspect of this broader discussion, a grid search algorithm is employed to explore potential grid and BESS combinations and determine the optimal solution. Moreover, the integrated BESS is scheduled for (dis)charging via linear programming (LP) to ensure that charging demands are fulfilled with minimal OE [10]. The use of real-world data regarding electricity dynamic prices (DP) and the demand profile of the UFCS ensures that this research remains grounded in practical and tangible scenarios. The implications of this paper extend far beyond monetary savings, as a well-managed BESS can improve grid stability.

We aim to provide a robust road map for harnessing the outreached potential of BESS in the rapidly evolving landscape of UFCS that can contribute to the sustainable development of e-mobility solutions. The rest of the paper is structured as follows: Section 2 presents a state-of-the-art related work. Section 3 elaborates on the Dutch energy market and energy pricing, and Section 4 presents the BESS modeling and aging. Section 5 illustrates the UFCS model, problem formulation, and optimization approach. Section 6 discusses the results, Section 7 presents the analysis and future projections of BESS, and Section 8 concludes the paper.

2. Related work

Undoubtedly, a clean and green transportation sector is one of the most promising ways to reduce greenhouse gas emissions. Achieving this goal is feasible if the energy used to recharge EVs comes from renewable energy sources (RESs). This paradigm shift towards a dual objective has increased EV growth and inverter-based resources (IBRs) penetration in power systems. However, due to the intermittent nature of IBRs and the impulsive charging demands of EVs, both act like a double-edged sword in the power system. Although, the network operators monitor and maintain the power system's stability and reliability parameters. However, any unbalanced and uncontrolled act in a UFCS or failure of a IBR can trigger a catastrophic failure. In this context, the ESS emerged as a viable solution and gradually became an integral part of the modern power system. Recently, numerous applications of ESSs have been reported, and various implementation methodologies have been proposed in the literature. Some of the most relevant literature is summarized hereafter.

Y. Wu et al. presented a real-time energy management system for a UFCS with integrated RES and ESS via direct load control [11]. The proposed strategy addressed a similar aim: to reduce reliance on the electric grid, reduce the impact of UFCS on the power system, and reduce charging costs. The formulated problem consists of homogeneous EV load and real-time energy prices and is solved via the convex optimization technique. Results illustrate that peak power demand is curtailed by 52.98% and charging costs are reduced by 31.7%. However, the assumption of homogeneous EV loads to simplify the problem is impractical, as each EV has a different battery capacity and characteristics. Moreover, the estimation of BESS lifespan and payback period are also excluded from the problem formulation.

To minimize the energy losses in the distribution network and reduce the charging costs of EVs with optimal power flow, an energy management strategy has been proposed in [12]. Various case studies have been conducted and tested on the IEEE 33-bus system to identify the optimal locations and sizes of UFCSs within the distribution network, incorporating distributed RES and ESS. An improved bald eagle search algorithm optimizes the energy dispatch to UFCSs and improves the buses' voltages. Instead of local ESS at the UFCS, the study tackled the problem from a distribution network perspective. It addressed the network stability and reliability issue but did not consider a built-in storage feature in UFCSs to reduce reliance on the electric grid.

Authors in [13] introduced a cluster-based approach for coordinated control of EVs in multiple UFCSs with integrated ESS. The paper considers an individual UFCS a microgrid and proposes a hierarchical control architecture for multiple UFCSs based on a 4G/5G communication network. The cluster-based approach has proven effective in responding rapidly to an imbalance in the regional power grid and ensuring power system stability. Moreover, similar methodologies for intelligent transportation systems based on the Internet of Things are also proposed in [14,15]. Y. Cao et al. present a publish and subscribe communication architecture for EVs; the roadside units are used as communications gateways between UFCSs and EVs [14]. The public transport buses are utilized as communication gateways instead of stationary roadside units in [15]. These studies share a common motivation to guide EVs towards less crowded UFCSs for coordinated charging. However, it can affect the seamless refilling experience of EV drivers as the battery's state of charge (SOC) is not included in the model to prioritize the charging.

Ref. [16] presents a cost-effective energy management system for UFCSs to recharge EVs based on energy prices. The formulated problem incorporated grid, ESS and RES capacities, and chargers' rating to maximize UFCS profit, and it is solved through mixed integer LP. This case study focuses on installing a UFCS on Piha Beach in New Zealand. The study claimed a profit of NZ$ 53,107 per annum with payback periods of less than two years. However, the economic model for payback period estimation, aging, and BESS degradation should be discussed in detail. Moreover, the study focused only on the level 3 DC 50 kW fast chargers, and the proposed model ignored the distribution network selection and integration criteria.

H. Tan et al. presented an optimization model for ESS integration into UFCSs [17]. The study incorporated capital investment, NO charges, grid connection, and ESS capacities to optimize the size of the ESS. Day-ahead and real-time energy prices are considered for the ESS dis(charging) and reducing charging costs. A similar optimization model is presented in [18]. In addition to ESS, this model also included the RES generation in the UFCS model. The proposed model is validated via numerical simulations, and results illustrate that investing in RES and ESS significantly reduced the UFCS annualized expenditures. However, these models should also consider the economic factors, including capital investments, the lifespan of the BESS, and the payback periods. To attract investors towards alternative charging infrastructure and expedite the energy transition with public–private partnerships.

Ref. [19] studied the implications of random and uncontrolled EVs' charging on the power system. A dynamic demand adjustment strategy is proposed while considering the integrated ESS and RES in UFCS. The multi-objective optimization problem is formulated and solved via a non-dominant sort genetic algorithm. Flexible constraints are imposed on the upper limit of ESS, which vary in response to load demand and real-time energy prices to utilize the RES-generated energy efficiently. Results show that this flexible configuration increases the use of RES in load sharing by 6% while the OE is reduced by 13% and grid

power fluctuations by 21%. However, the economic perspective, such as capital investments, BESS's lifespan and payback periods, should be considered in the model.

In [20], the authors presented the concept of ancillary ESS into the DC UFCSs. A Flywheel ESS (FESS) is integrated as a power buffer to provide power in the initial charging phase and avoid the impulsive burden on the grid. A similar research is also conducted in the [21]. The paper integrates FESS into UFCS to improve grid stability and mitigate power quality and voltage sag issues. The EV charging behaviors and corresponding impacts on the electric grid are analyzed via simulation, and the results are presented as a demonstrator for Austria's FlyGrid project. Although FESS has a speedy response time and long cyclic life, it can support EV charging to provide an initial burst of power for the short term and avoid the burdens on the grid. However, due to low energy density and high initial cost, FESS is unsuitable for UFCSs. Moreover, the economic perspective is ignored, and the network stability issue is addressed in both [20,21].

Authors in [22] proposed an alternative charging infrastructure model by integrating RES, ESS, and UFCS with the electric railway MV grid. The overhead catenary system transfers the RES-generated energy into UFCSs, and the integrated ESS works as an energy buffer to avoid burdening the railway grid in peak hours. The proposed model is appropriately designed, and the integrated load and resources are galvanically isolated from the rail network. Although using a railway-dedicated network for UFCSs is an exciting idea, it involves policy constraints and a proper load flow analysis to optimize ESS and RES locations.

3. DP and dutch energy market

To make UFCS business lucrative for the investors and expedite the energy transition via public–private partnerships. The OE, a combination of energy consumption (EC) and the network operator's (NO) charges, play a crucial role in UFCSs. According to the agreed set tariff (ST) or dynamic prices (DP) contract, the energy provider charges a UFCS based on actual EC consumed in kW-hour (kWh) during the billing period and the predetermined NO charges are based on connection size and sanctioned load. A BESS-integrated UFCS is a promising way to exploit the market condition to build an efficient demand and consumption model in the context of the Dutch energy market. Fig. 2 briefly illustrates the ESS categories and technologies [23], and we will focus only on the BESS in this paper.

3.1. Dutch energy market

In the Netherlands, about 44% of electricity connections have ST contracts [24]. According to the central bureau of statistics (CBS), the average price for industrial consumers with peak demand 2-to-20k MW was €0.156/kWh in 2023 [25]. The Dutch energy market also offers variable energy contracts and enables consumers to benefit from price fluctuations. The Netherlands market comprises three segments: day-ahead, intraday, and balancing markets [26]. In the day-ahead market, participants can sell or buy energy for 24 h in closed auctions. The intraday market allows market participants to trade continuously, 24 h a day. The primary goal of the balancing market is to maintain grid stability and respond quickly to unanticipated demand–supply imbalances. Prices in the day-ahead and intraday markets are usually determined in advance, whereas prices in the balancing market might fluctuate regularly and reflect real-time conditions.

The balancing market mainly consists of ancillary service providers and demand response aggregators. Fig. 3 comprehensively illustrates the ESS location, corresponding function, and its relation with RESs [23]. As shown in Fig. 3, market balancing, power system stability, and reliability functions are performed at the operator level in the transmission and distribution sections before the meter. The scope of this paper is limited to the consumer level and behind-the-meter part.

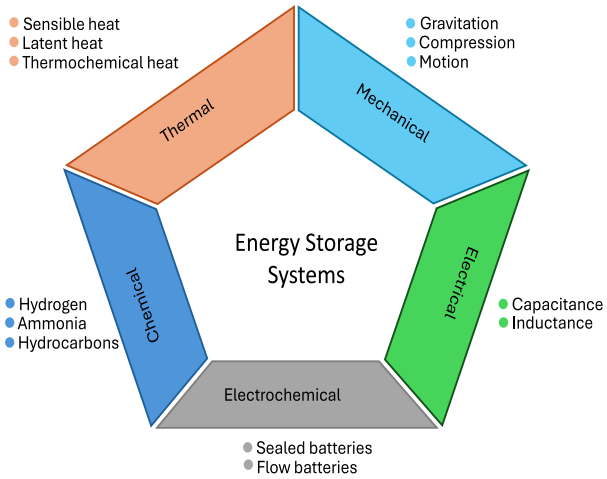

Fig. 2. Classification of ESSs based on storage technology [23].

Therefore, the day-ahead market is an exciting opportunity because prices fluctuate every hour while being known the day before, reducing OE by (dis)charging the BESS in response to energy prices. In our model, the UFCS is not an energy trader but can participate in charge reduction and backup power areas shown in Fig. 3.

3.2. Dutch NOs

In the Netherlands, several NOs provide services nationwide, charging consumers for infrastructure rather than electricity usage. These charges vary based on connection size, interfacing network, and connection category. For example, critical loads with reserve capacity (RC) requirements are charged more than non-critical consumers. Based on load demand and connection size, the connection is either provided from a residential LV distribution network such as ≤50 kW load or an MV distribution network with an MV/LV transformer (T/F) such as ≤150 kW load. The small-scale industrial or commercial consumers, e.g., ≥151 ≤1500 kW connections, are provided from the MV grid. Moreover, large-scale industrial connections such as >1500 kW are provided from the high voltage (HV) network directly or via HV/MV T/F. However, the NOs charge consumers for using infrastructure, including interfacing equipment, such as T/F charges. This study uses Stedin's tariffs as Stedin and FastNed stations (i.e., used for demand modeling) cooperate in the same region. Table 1 shows the NO's one-time connection and periodic maintenance charges. While Table 2 illustrates the fixed and variable charges of the energy transport to large-scale customers [27]. Variable fees change according to the maximum load drawn; therefore, integrating a BESS into the UFCS reduces direct reliance on the grid and NO expenses.

4. BESS modeling and aging

The choice of BESS technology influences the design and operational effectiveness of a UFCS integrated with a BESS. Lithium-ion (Li-ion) BESSs are well-known for their high round-trip efficiency, lifespan, and power and energy densities compared to their counterpart battery technologies. This section focuses on the mathematical modeling and aging of lithium iron phosphate (LFP) BESS due to its high lifespan and energy density, which makes it suitable for stationary applications [28].

4.1. Mathematical model

This model provides mathematical equations to describe the (dis) charging processes, considering internal and external temperatures,

Table 1
One-time and per connection fees of a grid connection [27].

Interfacing network	Connection size (kVA)	Annual charges (€)	One-time charges (€)	
			Connection	Cable/meter
LV	≥92 ≤ 143	122	5296	81
MV via MV/LV T/F	>143 ≤175	122	6528	85
MV	>175 ≤630	1092	25,059	152
MV	>630 ≤1000	1092	26,929	156
HV via HV/MV T/F	>1000 ≤1750	1092	75,470	302
HV via HV/MV T/F	>1750 ≤5000	2650	245,224	381
HV via HV/MV T/F	>5000 ≤10,000	13,099	328,114	429
HV	>10 000	Custom		

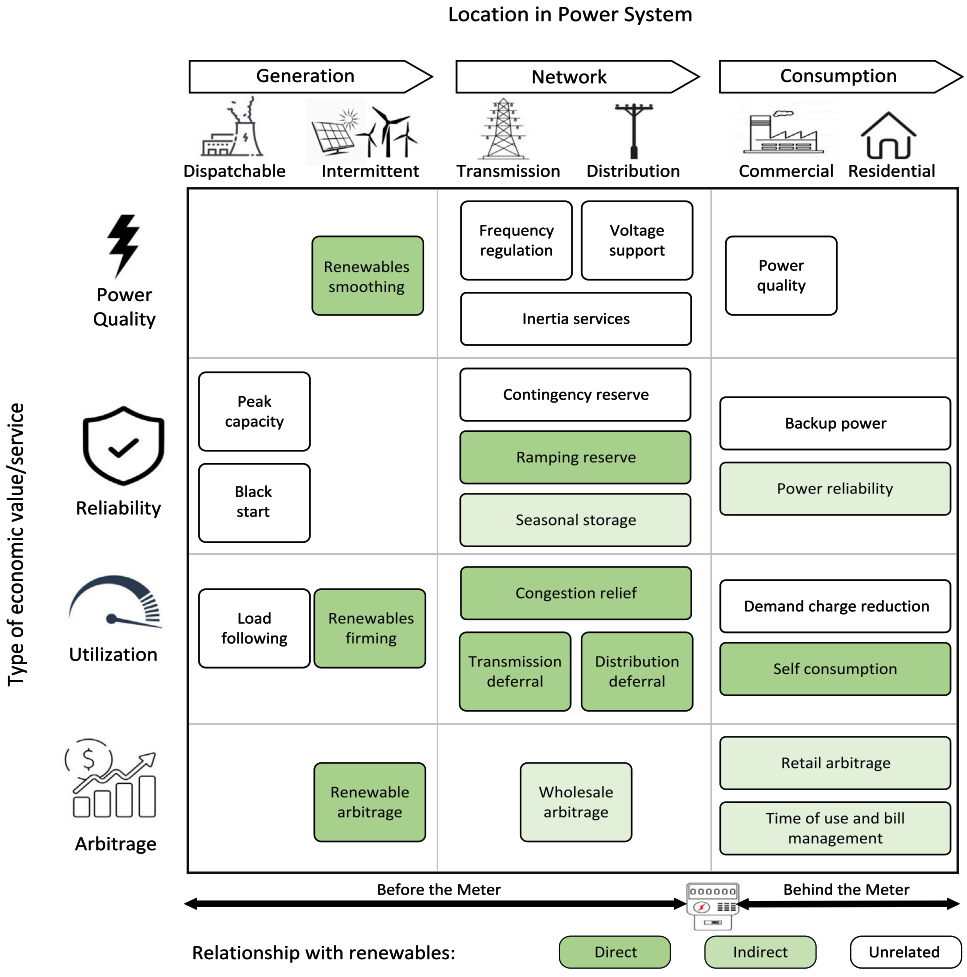

Fig. 3. An overview of the location and applications of ESSs in the power system [23].

Table 2
Variable energy transportation fees [27].

Interfacing network	Demand range (kW)	Standing charges (€/month)	Variable demand charges (€/month/kW)	
			Sanctioned	Peak
LV	≤50	1.50	1.18	–
MV via MV/LV T/F	51–150	36.75	3.17	2.43
MV	151–1500	36.75	1.61	2.43
HV via HV/MV T/F	>1500	230.00	1.52	1.41
HV via HV/MV T/F with RC	>1500	230.00	3.05	4.06
HV	>1500	230.00	1.47	1.39
HV with RC	>1500	230.00	2.94	4.02

BESS capacity, and voltage fluctuations. It also illustrates BESS performance across different temperatures and current conditions. Eq. (1) presents the current $i(t)$ at any given time t [29],

$$i(t) = \frac{P(t)}{V_b(t)} \tag{1}$$

where, $P(t)$ is input/output power and $V_b(t)$ is the BESS's terminal voltage at that time t.

A complex function f_{dis} determines the BESS's terminal voltage V_b during the discharge process while considering the effect of temperature, as given by Eqs. (2) and (3) [29],

Discharge Model $(i_l > 0)$

$$f_{dis}(c, i_l, i, T, T_a) = V_0(T) - K(T)\frac{Q(T_a)}{Q(T_a) - c}(i_l + c) + Ae^{-Bc} - Cc \tag{2}$$

$$V_b(T) = f_{dis}(c, i_l, i, T, T_a) - R(T)i \tag{3}$$

A similar approach, with minor changes, can be applied to the charging process as well and presented in Eqs. (4) and (5) [29],

Charge Model $(i_l < 0)$

$$f_{ch}(c, i_l, i, T, T_a) = V_0(T) - K(T)\frac{Q(T_a)}{c + 0.1Q(T_a)}i_l - K(T)\frac{Q(T_a)}{Q(T_a) - c}c + Ae^{-Bc} - Cc \tag{4}$$

$$V_b(T) = f_{ch}(c, i_l, i, T, T_a) - R(T)i \tag{5}$$

where c is the BESS's capacity in Ah, il is the low-frequency current dynamics, and i is the BESS's current in A, respectively. Similarly, T is the cell's temperature, and T_a is the ambient's temperature in $^\circ K$. Moreover, V_0 is the constant voltage in V, K is the polarization constant in V/Ah or polarization resistance in Ω, Q is the maximum BESS's capacity in Ah, e is exponential zone dynamics in V, A is the exponential voltage in V, B is the exponential capacity in Ah^{-1}, C is the nominal discharge curve slope in V/Ah, and R is the internal resistance in Ω.

The key temperature-dependent parameters required to accurately model BESS behavior under various thermal conditions are provided in Eqs. (6)–(9) [29],

$$V_0(T) = V_{0|T_{ref}} + \frac{\partial V}{\partial T}(T - T_{ref}) \tag{6}$$

$$Q(T_a) = Q_{|T_a} + \frac{\Delta Q}{\Delta T}(T_a - T_{ref}) \tag{7}$$

$$K(T) = K_{|T_{ref}} e^{\alpha\left(\frac{1}{T} - \frac{1}{T_{ref}}\right)} \tag{8}$$

$$R(T) = R_{|T_{ref}} e^{\beta\left(\frac{1}{T} - \frac{1}{T_{ref}}\right)} \tag{9}$$

where, T_{ref} is the nominal ambient temperature in $^\circ K$, and $\frac{\partial E}{\partial T}$ is the reversible voltage temperature coefficient in V/K. α and β are the Arrhenius rate constants for the polarization and internal resistance, respectively. $\frac{\Delta Q}{\Delta T}$ is the maximum capacity temperature coefficient in Ah/K.

The thermal power loss P_{tl} in W during the (dis)charge process is calculated by Eq. (10), and the internal temperature T at any given time t is given by Eq. (11) [29],

$$P_{tl} = (V_0(T) - V_b(T))i + \frac{\partial V}{\partial T}iT \tag{10}$$

$$T(t) = \mathcal{L}^{-1}\{\frac{P_{tl}}{\varrho} + \frac{T_a}{1 + \sigma\Gamma}\} \tag{11}$$

where, ϱ is the thermal resistance in $^\circ C/W$, σ represent the status of battery (dis)charging $\sigma = (0)1$ and Γ is cell to the ambient thermal time constant in s.

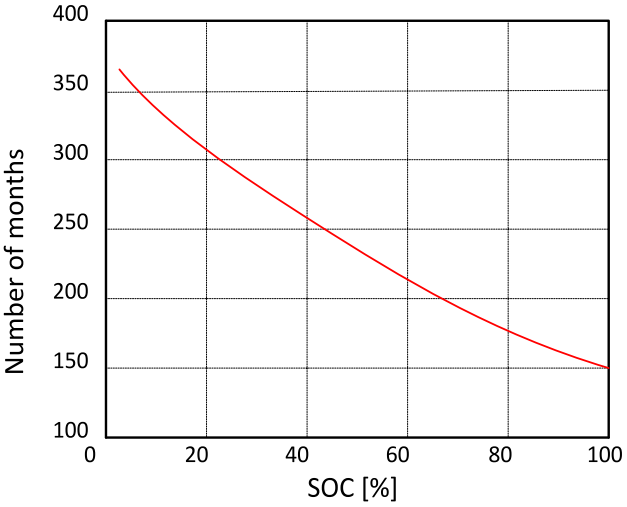

Fig. 4. LFP BESS calendar lifetime characteristic at 25 °C w.r.t. SOC [30].

This model ensures that real-world batteries can replicate the empirical model results by considering voltage changes and the SOC due to (dis)charging. This method validates the empirical model's reliability and allows accurate BESS deterioration and aging calculations. MATLAB Simulink is used to evaluate the model using inputs such as the (dis)charge power profile, cycle aging characteristics, initial BESS voltage, BESS capacity, and ambient temperature considered as 25 °C.

4.2. BESS degradation

The efficiency of a BESS in reducing the OE of a UFCS is directly related to its lifespan. Li-ion BESSs are prone to calendar and cycling degradations and have a significantly high lifespan.

4.2.1. Calendar degradation

The two main impactful factors that influence the calendar life of a Li-ion BESS are time and temperature. The high temperature causes parasitic reactions, increases internal resistance and creates a thicker solid electrolyte interphase (SEI) layer [31]. Additionally, the high utilization and high SOC for extended periods further worsen the effect of high temperature. The internal resistance also increased with time, and in the aged batteries, the deteriorated electrolyte and intrinsic electrode materials reduced the BESS capacity. Daniel et al. estimated the lifetime of Li-ion batteries using various SOCs, cycle depths and (dis)charging procedures to provide primary frequency response services, [32]. Moreover, a constant ambient temperature at 25 °C and an average of 50% SOC is considered to account for (dis)charge cycles. The estimated calendar lifetime declines exponentially in response to rises in idling SOC level [33], as given in Fig. 4 [30]. A linear regression model estimates that 20% capacity loss or EOL occurred in 8.5-to-13.5 [30]. With a 90-to-100% SOC usage, capacity losses climb dramatically, and an optimistic projection of Calendar lifespan is slightly more than 12 years [34–36].

4.2.2. Cycling degradation

The (dis)charging process of Li-ion BESSs causes cycling degradation and impacts the total lifespan. However, regulated (dis)charging processes allow more control over the aging rate. Factors such as voltage, high currents, depth of discharge (DD), and electrolyte oxidation cause cyclic degradation. High currents result in uneven electrode usage, discrete hot spots and expedited deterioration. DD puts stress on electrodes and leads to mechanical deterioration. Electrolyte oxidation, especially at high voltage levels, evaporates electrolytes and produces gas that may lead to potential rupture or leakage. Moreover, side

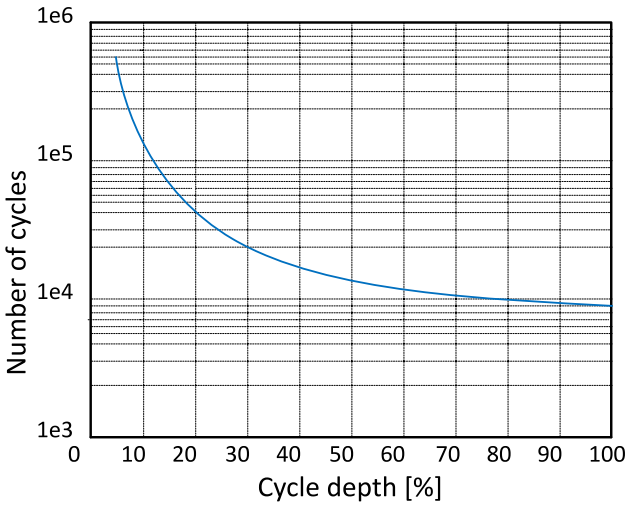

Fig. 5. LFP BESS cycling lifetime characteristic at 25 °C w.r.t. DD [30].

Table 3
LFP BESS cycling lifetime characteristic at 25 °C w.r.t. DD and number of cycles [32].

DD	Number of cycles
25%	60.000
50%	22.000
75%	15.000
100%	9.000

reactions boost internal resistance and reduce cell capacity. However, a sophisticated control of temperature, charging voltages, and DD can mitigate these degradation pathways [37]. To analyze the impact of cycle depth on lifetime, 70-to-90% of cycle depths, i.e., 5-to-95%, 10-to-90%, and 15-to-85% SOCs, were analyzed in [30,32]. Furthermore, an increase of eight months in lifespan is found with 70% cycle depth usage instead of 90%.

Conventional cyclic aging methods use the cyclic life vs. DD curve and provide cyclic life against a constant DD rate in (dis)charge processes, as shown in Fig. 5 [30]. The graph displays the maximum cycle depth for which an LFP battery can be used before it reaches the end-of-life (EOL), i.e., 80% of the rated capacity, as summarized in Table 3 [32]. This approach must be more complex; it ignores capacity loss per cycle, EOL's capacity, cell voltages, currents, and internal temperatures. A model that includes dynamic currents, voltages, DD, and temperature to accurately estimate cyclic aging of LFP batteries, particularly for UFCS applications that involve high capacities and capital costs.

4.3. Aging model

A model that calculates the effective lifespan of an LFP BESS and considers maximum capacity Q and internal resistance R at the beginning of life (BOL) and EOL is presented here [28]. Its comprehensive structure and account for (dis)charge processes, cycling degradation, and voltage swings make it a promising choice for estimating the lifespan of the integrated BESS. Moreover, it uses a cycle-by-cycle approach, and each (dis)charge cycle corresponds to a half-cycle duration of h in s. The capacity and resistance after each cycle n are calculated using the aging factor $\epsilon(n)$, as given by Eqs. (12) and (13) [29],

$$Q(n) = \begin{cases} Q_{bol} - \epsilon(n)\left(Q_{bol} - Q_{eol}\right) & \text{if } \kappa/2 \neq 0 \\ Q(n-1) & \text{otherwise} \end{cases} \tag{12}$$

$$R(n) = \begin{cases} R_{bol} + \epsilon(n)\left(R_{eol} - R_{bol}\right) & \text{if } \kappa/2 \neq 0 \\ R(n-1) & \text{otherwise} \end{cases} \tag{13}$$

where Q_{bol} and Q_{eol} are maximum capacities in Ah, and R_{bol} and R_{eol} are internal resistances in Ω at the BOL and EOL at nominal ambient temperature, respectively. While $n = \kappa h$ and $\kappa = 1, 2, 3.....\infty$.

The aging factor $a(n)$ accounts for the DD and the maximum number of cycles $N(n)$, is given by Eq. (14) [29],

$$\epsilon(n) = \begin{cases} \epsilon(n-1) + \frac{0.5}{N(n-1)}\left(2 - \frac{DD(n-2)+DD(n)}{DD(n-1)}\right) & \text{if } \kappa/2 \neq 0 \\ \epsilon(n-1) & \text{otherwise} \end{cases} \tag{14}$$

The dynamic value n is updated after each cycle based on the DD and maximum number of cycles N. The maximum number of cycles $N(n)$ is influenced by several factors, as given by Eq. (15) [29],

$$N(n) = H\left(\frac{DD(n)}{100}\right)^{-\xi} \mathrm{e}^{-\psi\left(\frac{1}{T_{ref}} - \frac{1}{T_a(n)}\right)} \left(\overline{I_{dis}}(n)\right)^{-\gamma_{dis}} \left(\overline{I_{ch}}(n)\right)^{-\gamma_{ch}} \tag{15}$$

where, H is cycles number constant, ξ is exponential factor of the DD, ψ Arrhenius rate constant for the cycles number, $\overline{I_{dis}}(n)$ and $\overline{I_{ch}}(n)$ are average (dis)charge currents in A for a half-cycle duration. Similarly, γ_{dis} and γ_{ch} are exponential factors for the (dis)charge currents.

This model is used to calculate the lifespan of integrated BESS with (dis)charge profiles optimized for OE reduction before it reaches EOL. The EOL criteria for LFP BESSs is 80%, which means a LFP battery retired at 80% of state of health (SOH) [38,39].

5. UFCS model, demand dynamics, problem formulation and optimization

This section outlines the UFCS model, charging demand dynamics, problem formulation, and optimization approach. The UFCS includes a BESS, grid connection, and power conversion units. A 1C-rated BESS with a temperature control system designed to maintain a stable temperature of 25 °C for enhanced performance is considered. The cost and energy consumption of the temperature control system are excluded from the calculations due to their minimal impact.

5.1. UFCS model

AC and DC common bus architectures of a UFCS offer unique advantages and disadvantages. The grid supplies AC power to the UFCS, while BESS and EVs require DC. Therefore, an AC bus architecture offers seamless integration with the electric grid with integration costs. It is well-suited for UFCSs with substantial AC loads, and an MV/LV distribution transformer interfaces the grid and creates a common bus. The EV chargers, ESS and RES, are connected to the AC bus via AC/DC and DC/AC power converters. However, this configuration leads to inefficiencies and energy losses, especially in DC-centric loads like EVs and BESS.

In contrast, a DC bus configuration provides significant advantages for UFCSs, such as higher efficiency and seamless integration of EV, BESS, and RES. However, it brings challenges like higher costs and increased control complexities compared to the AC bus system, but it remains a promising option for UFCSs. Proper galvanic isolation between the grid and the UFCS is essential to prevent fault transfer between AC and DC networks, as documented in [41–43]. Therefore, isolated DC/DC converters connect EV chargers to a common DC bus to provide electrical isolation and magnetic coupling for power flow. AC/DC rectification, power factor correction, and voltage regulation are also crucial components of a DC bus architecture.

Besides its limitations, the DC common bus architecture is the most reliable and efficient configuration for UFCS to integrate the inherent DC load and sources at one common point. Fig. 6 illustrates the UFCS's schematic and a solid-state transformer (SST) symbolizes the power conversion stage (PCS). The SST provides galvanic isolation and maintains a regulated voltage via DC/DC converter [40]. Under soft-switching conditions, the efficiencies of the SST and DC/DC converters are 91-to-98% and 99%, respectively. The round-trip efficiencies of

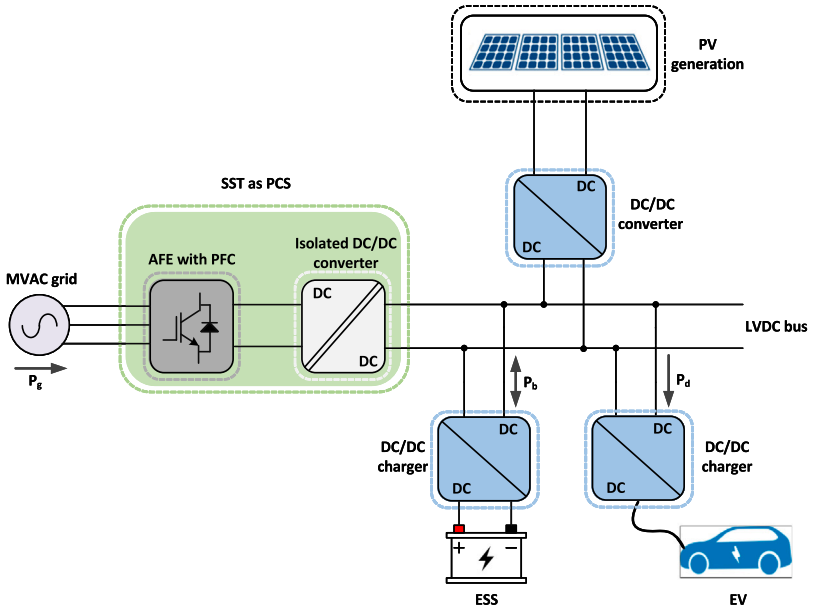

Fig. 6. Schematic of a BESS-integrated DC-bus UFCS [40].

Table 4
Efficiencies of power electronic components and LFP BESS [44,45].

Efficiency	Power electronic components		LFP BESS
	PCS	DC/DC convert	
Range	91-to-98	99%	94-to-98%
Estimated	95%	99%	96%

Table 5
Cost estimation of power electronic components [47].

Cost (€/kW)	PCS	Misc	DC/DC converter
Range	184-to-239	75–115	69-to-130
Estimated	211	95	100

LFP BESS also lie between 94-to-98% as given in Table 4 [44,45]. Moreover, the investment in PCS and DC/DC converters depends on grid connection and BESS sizes. A UFCS with a sufficient grid connection and a smaller BESS requires a more prominent PCS and a smaller DC/DC converter, resulting in high PCS and miscellaneous (Misc) investments and small DC/DC converter costs, and vice versa. Table 5 provides range and estimation of the costs for power electronics components [46–48].

5.2. Charging demand dynamics

To determine the size of BESSs for integration with UFCSs, it is crucial to include two key factors: demand profile and chargers' utilization factor. Demand predictions and forecasts using historical data via statistical models and algorithms are well-reported in the literature [49–52]. This paper models daily, weekly and monthly demand profiles based on FastNed data [7,8] and [49–55].

The design and manufacturer's specifications impact EVs' charging behaviors, and every EV poses a distinct behavior. To prevent overcharging and battery degradation, the battery management system of EV reduces charging speed as the SOC reaches the 80% threshold, and on average, 60% recharge per session of 10 min is considered fast charging [52,56]. The EV's battery capacity is an essential factor that influences the demand profile and charger utilization. Although some EVs have over 100 kWh batteries, the average is around 50-to-60 kWh, and combined with SOC and charging rate, the recharge time is determined.

Besides individual EV charging dynamics, certain factors such as weekdays, weekends, weather patterns, seasonal mobility and station location impact the charging demand and dynamics of UFCSs. Studies indicate high charging demands on weekends for UFCSs located on highways. However, UFCSs in urban areas show the opposite trend, as most of the EVs in cities are used for short commutes, and high demand occurs on weekdays rather than weekends [49–52].

Using the FastNed data that shows a 50% utilization in peak hours and 20% in off-peak hours to estimate the hourly utilization factor for a UFCS [7,8,49–55]. The charging demand dynamics are incorporated into the model to generate daily, weekly and monthly load profiles of the UFCS.

5.3. Problem formulation

The aim is to reduce OE and reliance on the electric grid to address network congestion and contribute towards sustainable transportation. Furthermore, to ensure the stable operation of UFCS with improved (dis)charging efficiencies and better BESS's lifespan. The optimization problem is formulated and presented here.

Although EVs' charging requirements in real-world scenarios depend on SOC, model specifications, and user preferences. This paper considers specific charging speeds for EVs with homogeneous batteries of 60 kWh and charging demand from 20-to-80% SOC to maintain a streamlined approach. A UFCS is designed to offer charging speeds of 50, 175 and 350 kW per charger. The analytical energy and supply–demand balancing models are covered hereafter.

Power demand, the critical aspect of this problem formulation, is given by Eq. (16),

$$P_d(\tau) = \sum_{P_c=50}^{350} \sum_{j=1}^{19} \sum_{\tau=1}^{144} P_{ev}(P_c, j, \tau) \tag{16}$$

where $P_d(\tau)$ represents the total power demand at time instant τ, P_{ev} is the amount of power delivered to EVs, P_c is the power rating of chargers, j is the number of chargers, and τ indicates the number of time slots (i.e., 10 min per slot) per day.

To include the BESS in problem formulation and maintain supply–demand balance, the total power demand is expressed as an equality constraint in Eq. (17),

$$P_d(\tau) = P_g(\tau) \cdot \eta_g + k \cdot \eta_b^k \cdot P_b(\tau) \tag{17}$$

where, $P_g(\tau)$ is the available grid power at time τ, η_g represents PCS efficiency, η_b denotes the BESS conversion efficiency, $k = 1, -1$ demonstrates the (dis)charging status, and $P_b(\tau)$ is the power stored(released) by the BESS at time τ.

The Eq. (17) is subjected to the equality and inequality constraints given by Eqs. (18)–(20),

$$0 \leq P_g(\tau) \leq P_{gmax} \tag{18}$$

$$-P_{bmax} \leq P_b(\tau) \leq P_{bmax} \tag{19}$$

$$E_{bmin} \leq E_b(\tau) \leq E_{bmax} \tag{20}$$

where, Eq. (18) is the constraint imposed on the grid power P_g that restricts it to $\leq P_{gmax}$. Similarly, the (dis)charging boundaries of power release (absorb) by BESS are set to P_{bmax} and $-P_{bmax}$. While the BESS SOC, i.e., $E_b(\tau)$ at time τ,has limitations of E_{bmax} and E_{bmin}, respectively.

Moreover, the SOC of BESS and power released(absorbed) is given by Eq. (21),

$$E_b(\tau) = E_b(\tau - 1) + k \cdot \sum P_b(\tau) \cdot \zeta \tag{21}$$

where $E_b(\tau - 1)$ shows the previous SOC, $P_b(\tau)$ is the power release(absorb) by BESS in the current time slot τ, and $\zeta = \kappa\tau$ is the number of slots for which the BESS remains in (dis)charging state, and k shows the (dis)charge status.

MATLAB model generates a 30-day demand profile for high-speed charging sessions to validate the developed scenarios. The proposed UFCS consists of 50-to-350 kW chargers with a cumulative charging demand of 3.5 MW. Moreover, the power demand of six 350 kW, six 175 kW, and seven 50 kW chargers with charging durations of 10, 20, and 70 min, respectively, is met by a 1 MW grid connection and a 2.5 MWh BESS.

5.4. Optimization algorithms

An optimization problem with multiple variables and constraints requires careful selection of the optimization approach. Here, we discuss the best-suited optimization methods for the optimization objective and problem formulated earlier.

Grid search algorithm is a fundamental optimization technique that involves a systematic and exhaustive exploration of the given parameter space [57]. It assesses and evaluates all the possible combinations in the predefined set of parameter spaces to find the combination that provides the best performance for the model. This brute-force approach achieves outstanding precision and is suitable for multi-parameter optimization problems [58]. In our optimization problem, grid search is cleverly used to investigate two critical parameters: grid and BESS capacities. Each parameter fluctuates in predetermined values of 0-to-3.5 MW, creating a multidimensional grid of possible combinations. Therefore, the grid search algorithm is well-suited to find optimal grid and BESS capacities and corresponding OE, further explained in Section 6.3.

By describing the objective function and constraints as linear equalities or inequalities, LP simplifies problems but applies only to linearized or inherently linear issues [59]. Our formulated problem is intrinsically linear, with the objective function being cost minimization and constraints being energy balance, BESS (dis)charge limits, and maximum grid capacity. So, LP is used to optimize the (dis)charging processes of the optimal size BESS found via the grid search algorithm. Moreover, the most suited LP strategy for BESS scheduling is the dual simplex (DS) algorithm because it cares for minor constraints that may render the current solution infeasible [60]. Despite potential infeasibilities caused by dynamic constraints, the DS approach stays durable and ensures optimization as the parameters grow. Other LP techniques, such as the interior-point approach, are suitable for large-scale problems but must be adjusted for dynamic constraints [61]. The dynamic nature of the formulated problem and evolving limitations favor the DS technique.

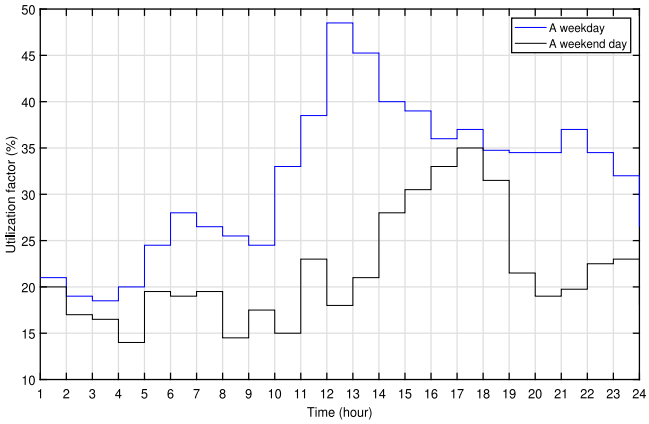

Fig. 7. Data-based: utilization factor (%) on an hourly basis [7,8,49–55].

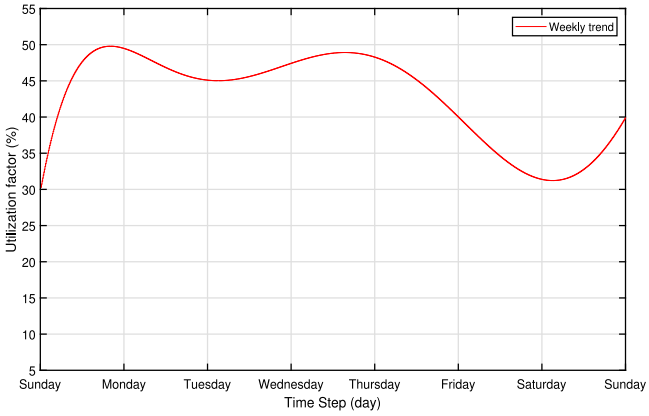

Fig. 8. Model-based: weekly utilization factor (%).

6. Results and discussion

This section summarizes the results, evaluates promising scenarios, analyzes demand profiles and OE with(out) BESS and elaborates on the optimal case study. Moreover, it calculates lifetime payback periods and investigates the merits of BESS integration.

6.1. Utilization factor

To compare the model's utilization factor with FastNed and literature data. The normalized utilization factor of FastNed stations in Hoogendoorn, Knorrestein, Elstgeest, Maatveld, and de Vink stations is presented in Fig. 7 [7,8,49–55]. Each station has 9-to-12 charging slots with 50-to-350 kW EV chargers. Fig. 7 indicates a high utilization factor of around 50% on weekdays due to work routine [7,8] and [49–55]. Moreover, the trend is reduced on the weekend as EVs are primarily used for short commutes in the cities; it is also aligned with the literature occupation peak of 35%. However, it is subjected to daily, weekly and seasonal changes, and UFCSs located on the highways may experience different utilization factors [49–52].

The computed trend line presented in Fig. 8 has several similarities with the utilization factor shown in Fig. 7, such as amplitudes and times of peaks that coincide. The likelihood that an EV driver can opt for 50, 175, and 350 kW charging speeds is equal, so only in the worst case a high utilization factor can cause high power demand. As mentioned earlier, the charging trend is subjected to numerous

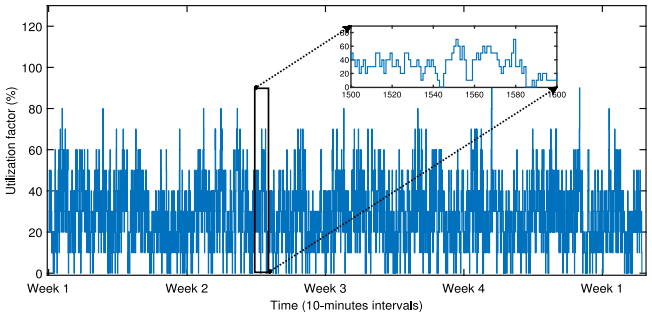

Fig. 9. Model-based: monthly utilization factor (%).

Table 6
Yearly OE (k€) per configuration.

BESS (MWh)	Grid connection (MW)							
	0.5	1	1.5	2	2.5	3	3.5	4
0.5		–	–	461	486	501	519	538
1		–	349	449	478	496	512	532
1.5		317	340	439	482	514	532	550
2		311	333	431	474	517	551	569
2.5	–	**307**	327	426	468	510	553	590
3		307	323	422	463	506	548	591
3.5		307	321	419	461	503	545	587
4		310	321	417	459	501	543	585
4.5		313	322	417	458	500	542	584

variations; a comprehensive utilization factor for a month is given in Fig. 9. The modeled UFCS has 21 charging slots of six 350 kW, six 175 and seven 50 kW chargers. It is important to note that the highest simultaneous charging of nine EVs occurs, and the per-month co-charging remains at three.

6.2. Power demand evaluation & DP

The daily and weekly demand profiles are accumulated and evaluated on a 30-day billing period basis to optimize the model's performance. The arrival and departure times of EVs, the charging duration, the opt-for charging speeds and charging slots utilization factor, the power demands of the 50-to-350 kW chargers category, and the cumulative power demand of UFCS are analyzed. Apart from the results shown in Fig. 10, the UFCS must be capable of handling the worst-case scenario of 3.5 MW of peak power demand. Fig. 10 depicts the power demand dynamics for 50-to-350 kW charging speeds. The x-axis time interval (i.e., 10 min) is calculated using a 350 kW charger as a reference that refills a 60 kWh battery in approximately 10 min. The daily, weekly, and monthly charging slots are 144, 1008 and 4320, respectively, as shown in the zoomed window. Moreover, Fig. 10(a)–(c) demonstrate the power demand of 50, 175 and 350 kW chargers categories, while Fig. 10(d) depicts a cumulative power demand of a 30-day billing period of the UFCS.

Despite the slow charging rate, 50 kW chargers have shown high utilization and occupancy. Around the 16th day, Fig. 10(a) depicts a peak of 0.3 MW; otherwise, the monthly average remains at 0.1 MW. Fig. 10(b) illustrates the power profile of 175 kW chargers; compared to 50 kW charges, it creates high peaks. Moreover, simultaneous charging sessions of four EVs created a peak of 0.7 MW. Fig. 10(c) shows the demand dynamics of the 350 kW chargers category. The high power demand of this charging speed creates a significant peak, and a co-charging session of three EVs generated a peak of 1.05 MW. In addition, Fig. 10(d) presents the cumulative power demand of UFCS for a one-month billing period, and it influences the decisions regarding grid connection, BESS sizes and the scheduling of BESS.

The UFCS's peak power demand remains at 1.75 MW, i.e., 50% of the maximum theoretical capacity and shows a 50% utilization factor of charging slots. However, it is subjected to variations due to UFCS location, on-road EVs and charging behaviors. A combined grid and BESS capacity of 3.5 MW is required to meet the maximum power demand in the worst-case scenario.

6.2.1. Implications of DP

A comparison of ST and DP is provided here to highlight BESS's importance in reducing UFCS's OE by storing low-price energy for later use. Fig. 11 depicts the ST and DP obtained from the Estone transparency platform for January and July 2023 [62]. One important thing to note is the average summer and winter prices, i.e., €0.07/kWh and €0.13/kWh, respectively, and the yearly average of €0.10/kWh of DP remains significantly less than €0.156/kWh ST. However, irregular peaks such as €0.30/kWh may raise OE if they coincide with peak demand. The demand profile shown in Fig. 10(d), the peak power demand coincides with DP fluctuations and results in a 24% reduction from €706k to €535k in annual OE, as shown in Fig. 12.

Moreover, the ST and DP are compared here in the absence of BESS, and the €535k per annum OE in the case of DP without BESS is a base case for further results and discussions such as Section 6.3 and Fig. 13.

6.3. Optimization assessment & global optimal solution

Fig. 13 demonstrates the persuasiveness of the grid-searching optimization algorithm, which generates several feasible combinations of grid connection size and BESS capacity to fulfill the 3.5 MW load demand. Each point represents a local optimal solution, and the global optimal solution can be identified based on the objective function, i.e., reduced OE with 3.5 MW capacity. The z-axis in Fig. 13(a) represents the corresponding OE, while in Fig. 13(b), it illustrates the reduction (%) in OE for each sub-optimal solution. The base case of 3.5 MW load demand and corresponding €535k per annum OE with DP is used to calculate OE and reduction (%) in OE at each point.

6.3.1. Global optimal solution

In order to identify the global optimal solution among the feasible combinations of grid and BESS that ensure the fulfillment of 3.5 MW load demand with minimum OE, local optimal solutions of Fig. 13(a) are tabulated in Table 6. It illustrates that the feasible region lies between 1-to-3.5 MW grid connection and 2.5-to-0 MWh BESS sizes. A grid connection below 1 MW is infeasible mainly due to increased operation and maintenance (O&M) expenses and reduced power availability to charge the BESS. Moreover, a 1 MW grid connection and 2.5 MWh BESS capacity with approximately €307k per annum OE is the global optimal solution among all feasible combinations.

Furthermore, Fig. 14 illustrates the per annum OE of five feasible configurations of grid connection size and BESS capacity under ST and DP environments. As discussed earlier and presented in Fig. 12, DP is more beneficial than ST. However, the global optimal solution of a 1 MW grid connection and 2.5 MWh BESS capacity further enhances the UFCS potential to store energy for later use. This combination leads to 57% less or saving €399k and 42% less or saving €280k in annual OE than without BESS scenarios under ST and DP, respectively.

Besides the reduced OE, the global optimal solution also reduced the interconnected aspect of the OE, i.e., PAR. The 2.5 MWh BESS with a 1 MW grid connection solution results in 73% reduced PAR. It indicates that fluctuations in the demand profile are reduced, and limited resources are efficiently utilized.

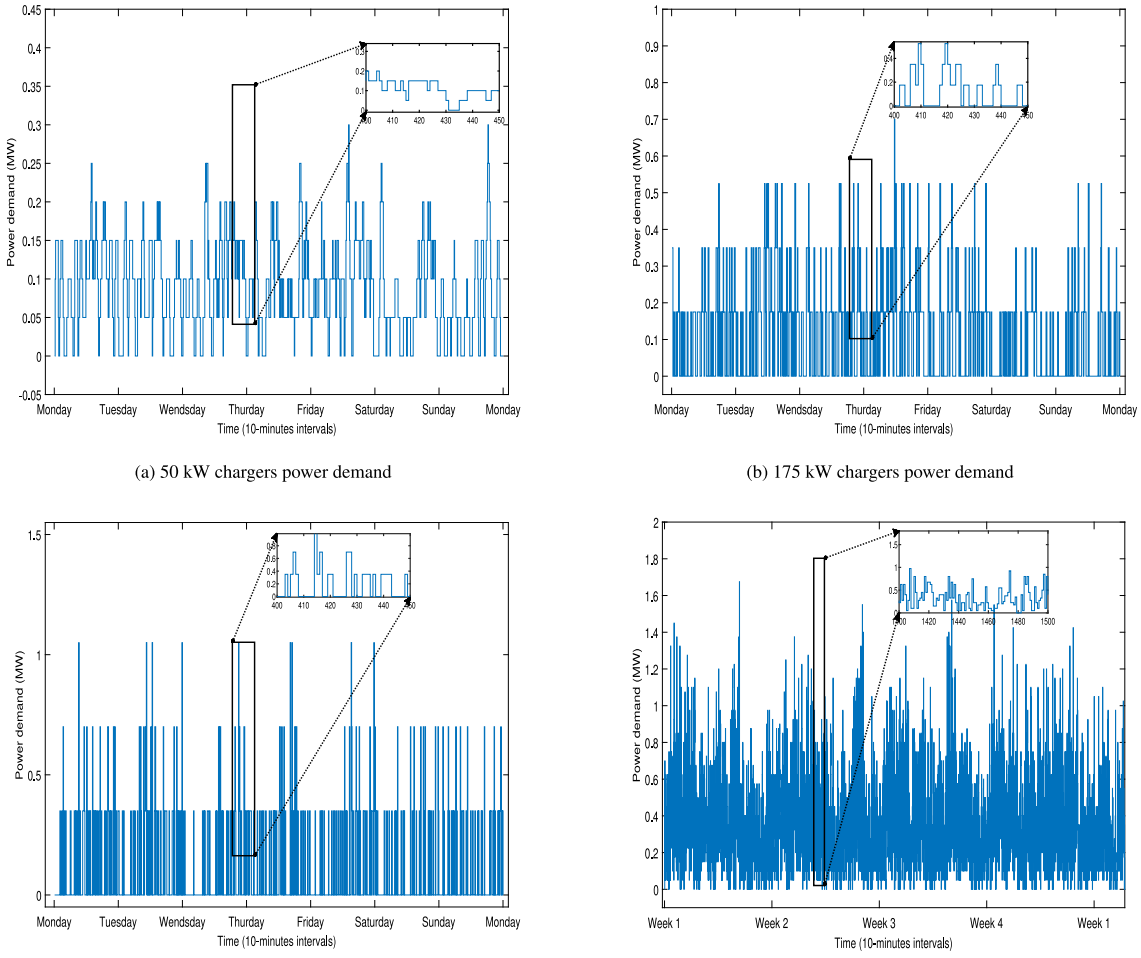

(a) 50 kW chargers power demand

(b) 175 kW chargers power demand

(c) 350 kW chargers power demand

(d) Cumulative power demand

Fig. 10. Model-based: 50-to-350 kW chargers and cumulative power demand for 30 days.

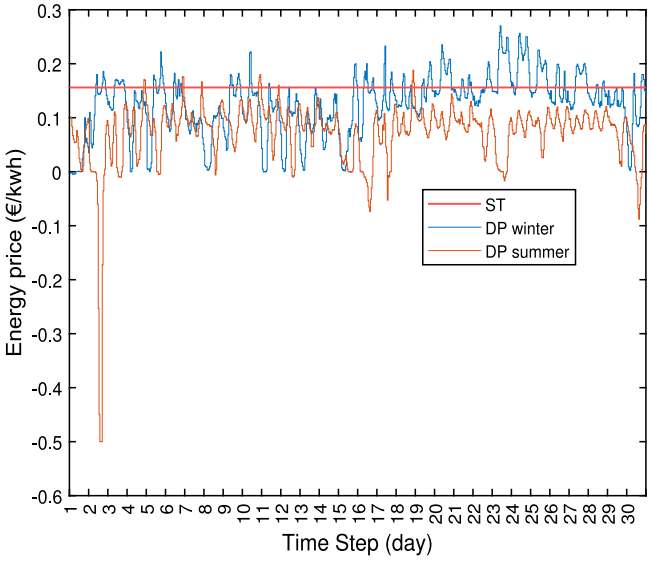

Fig. 11. ST and winter and summer DP [62].

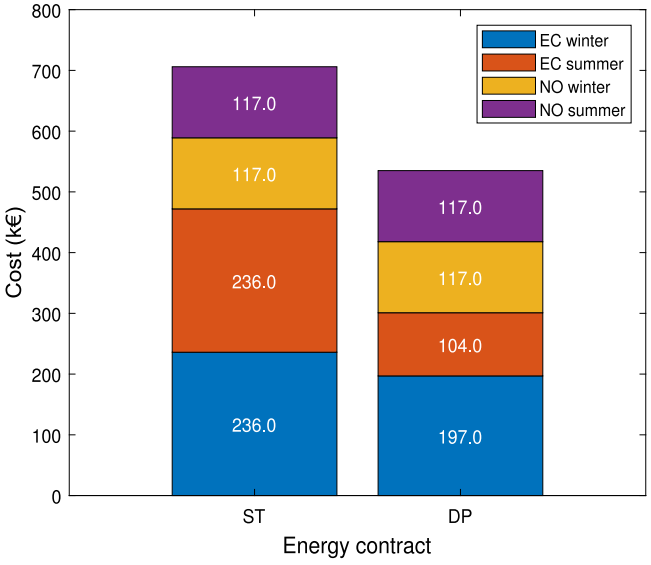

Fig. 12. Per annum difference between OE in case of ST and DP.

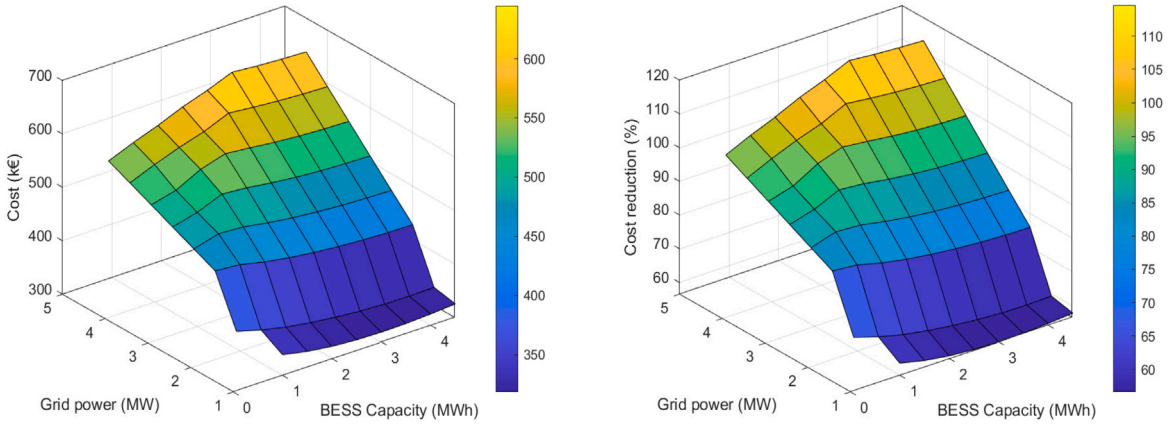

(a) OE (b) Reduction (%)

Fig. 13. Per annum OE and reduction in case of various grid and BESS configurations.

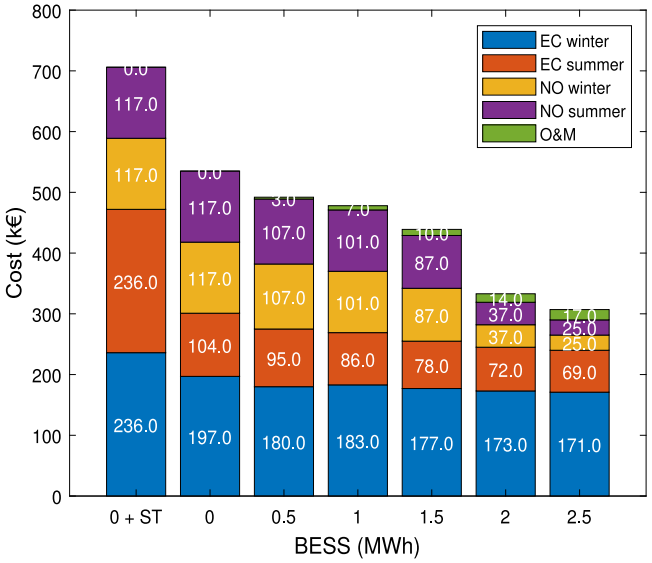

Fig. 14. Per annum OE of the feasible grid and BESS configurations.

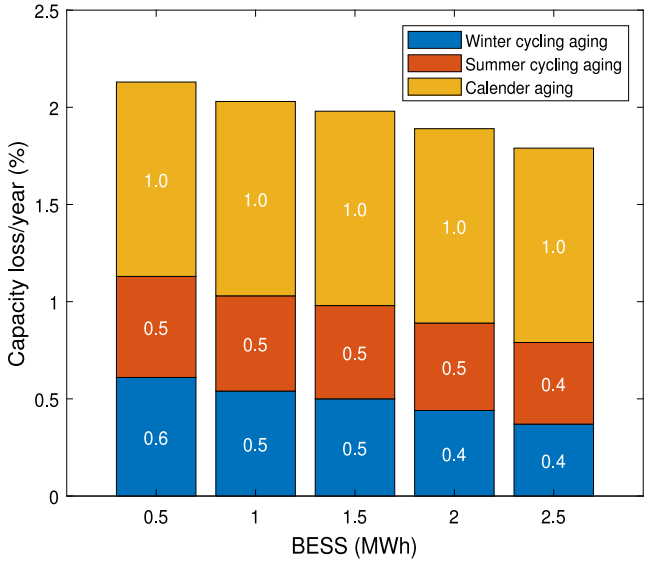

Fig. 15. Summer and winter cycling degradation (%) and calendar aging (%) for various BESS capacities.

6.4. Lifespan of BESS

Calendar and cycling degradations influence the lifespan of a BESS. Literature suggests a steady 1% capacity loss per year for calendar degradation. However, the cyclic degradation depends on (dis)charge cycles. The cycling aging model given in Section 4.3 is implemented in Simulink to estimate the capacity loss due to (dis)charge cycles. The estimated capacity loss in Ah by the Simulink model is translated from Ah to % of the original capacity, as presented in Fig. 15. It illustrates that cyclic aging reduces as BESS capacity increases. Using Fig. 15 results in combination with EOL and SOH, the 2.5 MWh BESS lifespan is estimated at 11.2 years.

6.5. Capital investment (CI), payback and profit periods

6.5.1. CI

The CI to design and implement a DC-bus BESS-integrated UFCS is influenced by several factors: (1) grid connection size, (2) PCS-rated capacity, (3) BESS-rated capacity, (4) cost of capacity (COC), (5) DC/DC converters, (6) cost of commissioning (CC), (7) O&M charges, and (8) Misc expenses.

Fig. 16 illustrates CI for five feasible solutions; at first glance, the CIs for all configurations look alike because the CI includes BESS and PCS investments. It is evident from Fig. 16 that without a BESS, CI does not include COC, CC, and DC/DC converters investments, and investment in PCS is significant. In the case of a 2.5 MWh BESS, the PCS investment is significantly reduced, but costs of COC, CC and DC/DC converters increased.

6.5.2. Payback period

The payback periods of BESS-integrated UFCSs can be estimated by considering OE reduction and required CI. UFCSs with 0.5-to-1.5 MWh BESSs and 3-to-2 MW grid connections have over one-year payback periods. However, configurations with 2-to-2.5 MWh BESSs show much smaller payback periods, mainly due to reduced grid connection size and related OE.

6.5.3. Profit period

The profit periods of BESS-integrated UFCSs can be derived from the BESS lifespan and payback period. The 0.5 MWh BESS and 3 MW grid configuration is proven profitable for 88% of its lifetime, and

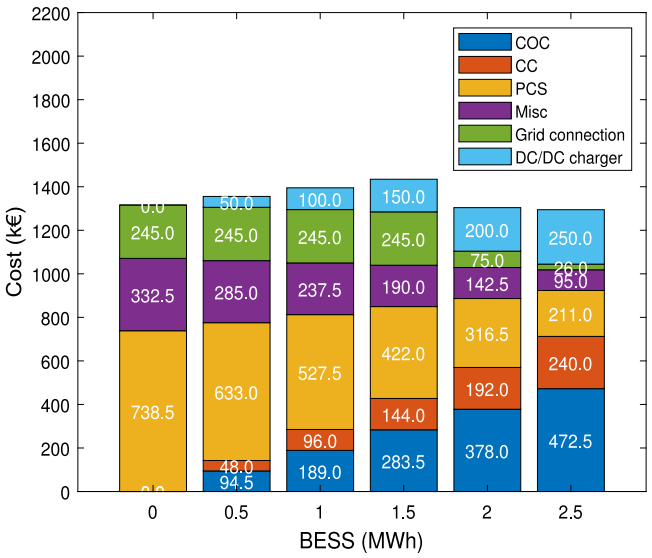

Fig. 16. The CI (including both PCS and BESS costs) is required for a 3.5 MW UFCS with 1 MW grid power and 2.5 MWh BESS.

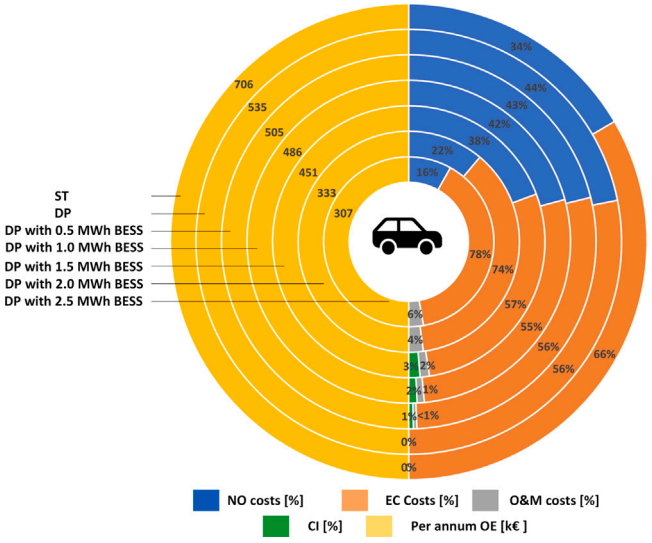

Fig. 17. The net reduction in various expenses over the lifetime of the BESS.

configurations with extensive BESS sizes have over 99% profit period and extended lifetime due to reduced dis(charge) cycles.

6.6. Net OE per annum

In the context of OE, a 3.5 MW UFCS with a minimum per annum OE is considered an optimal configuration. However, these parameters must be expressed per year over BESS's effective lifespan to include CI, O&M charges and BESS's lifespan in the equation with OE. Fig. 17 shows two half circles; the half circles on the left side present net per annum expenses in absolute values, and the half circles on the right side illustrate the share of NO, EC, maintenance, and CI in % in net per annum expenses. A steady decline is visible in OE as the BESS capacity increases. A 2.5 MWh BESS with a 1 MW grid connection in the DP environment reduces the net per annum expenses by 56%, from €706k to €307k.

Table 7
Comparison of initial and optimal UFCS configurations.

Evaluation parameter	Configuration	
	Initial	Optimal
Energy pricing	ST	DP
Grid connection (MW)	3.5	1
Maximum demand (MW)	3.5	1
BESS Capacity (MWh)	0	2.5
BESS lifespan (years)	–	11.2
EC expenses (k€)	470	240
NO expenses (k€)	334	50
O&M expenses (k€)	–	17
PAR reduction	–	73%
CI (k€)	1316	1294

6.7. Case study of optimal configuration

The optimal configuration of a 2.5 MWh BESS and a 1 MW grid power surpasses the initial configuration in terms of OE and PAR reduction, as summarized in Table 7.

Fig. 18 demonstrates the performance of optimal configuration with BESS and scheduling strategy for 72 h under the DP environment. Initially, the BESS is charged from the grid even in high-price slots. Afterward, the grid power is used in low-price slots to satisfy the UFCS demand, while the BESS offers assistance in high-price slots. Moreover, the charging demands are fulfilled irrespective of the energy prices if they exceed the grid capacity, as visible at the 42nd hour.

7. Analysis and future projections of BESS

BESS will be critical to meet the global carbon neutrality goal by 2050. Power and energy densities, lifespan, efficiency, and cost considerations determine the choice of battery technology for a specific application. For UFCS applications to incorporate RES, control PAR, and improve grid reliability, they require efficient, reliable, cost-effective BESS. Although Li-ion and LFP dominate the current market, they are under increasing scrutiny due to their over-reliance on crucial elements such as cobalt and graphite and their environmental consequences. Therefore, the future energy landscape requires broader diversification of storage chemistries with higher energy densities, longer lifetimes, faster charging, more safety, and economic sustainability. In this context, extensive research has focused on alternatives to traditional cathode materials, and emerging technologies like solid-state batteries have significant potential for future applications due to their outstanding specific and volumetric energy densities compared to Li-ion and LFP batteries [63].

Among the current and evolving technologies, the most relevant batteries include Li-ion, LFP, sodium-ion, flow, solid-state, lead–acid, and zinc-based batteries. Table 8 presents a comparative analysis of these battery technologies to identify their suitability for UFCS applications. Despite high prices and limited commercialization, solid-state batteries are emerging as a promising alternative to LFP batteries for stationary applications due to ultra-high energy density and extended lifespans. Based on their energy densities, lifespans, and efficiencies, solid-state batteries will be an ideal candidate for the next generation of charging infrastructure.

8. Conclusion

The exponential growth in on-road EVs increases the demand for alternative charging infrastructure. The impulsive power demand of EVs and the online connection of UFCSs bring significant challenges to the power system. Although the probability of co-charging is minimal due to multiple charger slots in UFCSs, simultaneous charging results in peak power demand and increased OE. To address this dual aspect of a UFCS, BESS is a compelling solution, and its integration into UFCSs

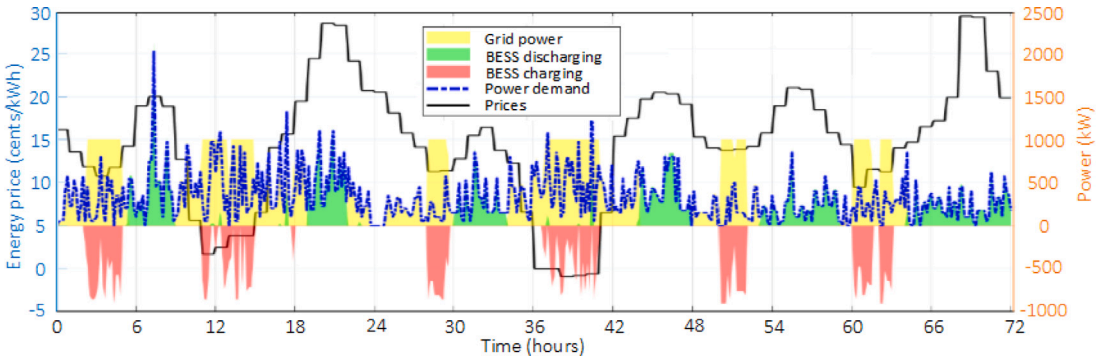

Fig. 18. An illustration of the energy flows for three days during the summer pricing period.

Table 8
A comparative analysis of current and evolving battery technologies.

Technology	Energy density (Wh/kg)	Lifespan (Cycles)	Efficiency (%)	Cost	Remarks
Li-ion	150–250	3000–5000	90–95	High	Suitable for peak shavings, prone to thermal runaway, and high costs.
LFP	90–160	7000–10,000	90–95	Moderate	Suitable for stationary applications, prone to lower energy densities.
Sodium-ion	90–150	2000–3000	85–90	Low-to-Moderate	Emerging technology for cost-sensitive and moderate-energy applications, but in the early stage of commercialization.
Flow batteries	20–40	10,000–20,000	65–80	High	Suitable for seasonal storage, offers an extremely long lifespan but is prone to very high CI and has low energy densities.
Solid-state	250–400	>10,000	90–95	Very high	Early-stage development for high-performance energy storage solutions, offer high energy density and extended longer lifespan, game-changer for next-generation charging infrastructure.
Lead–acid	30–50	500–2000	75–85	Low	Limited use in small backup power applications, a decline in usage.
Zinc-based	70–100	2000–10,000	60–80	Low-to-Moderate	In the experimental stage, environmentally friendly, potential low-cost alternative for stationary storage.

reduces reliance on the electric grid, minimizes OE and improves power system stability by curtailing the PAR.

This paper demonstrates an energy management system that integrates BESS into a UFCS and significantly enhances its techno-economic performance and feasibility. After evaluating and comparing critical characteristics, the day-ahead market has proven more effective even without a BESS than ST, resulting in a 36% reduction in EC expenditures. However, the unexpected arrival of EVs and changes in the energy market make it vulnerable and unpredictable without BESS. The integrated BESS significantly reduced reliance on the grid, i.e., up to 74% and efficiently tackled the net congestion issue while fulfilling charging demands with limited grid connection. Moreover, a 2.5 MWh BESS resulted in a 79% reduced NO due to the small grid connection. The benefits of DP in the day-ahead market include (dis)charging BESS in high and low price slots using LP to cut EC expenses. Compared to the situation without BESS and ST, the average cost/kWh is reduced by 49% in the BESS and DP situations. It reduces annual OE by up to 56%, demonstrating that a tailored optimization method effectively manages a BESS in a UFCS. The aging model shows a shorter lifespan due to high (dis)charge cycles. However, the BESS's life still exceeds the payback period and proves beneficial. The combination of 70% BESS and 30% grid capacities results in a 70% reduction in PAR and a 44% reduction in OE before BESS reaches EOL.

Besides reducing OE and reliance on the power system, integrating BESS into UFCSs can also bring significant opportunities. In the context of IBR penetration and the paradigm shift towards RES, the BESS-integrated UFCS will become valuable resources in the future power system. Implementing grid support and grid forming control techniques instead of the grid following will make UFCS a viable asset. These advanced control techniques provide frequency and voltage support services to the power system, rapidly respond to the generation-load imbalances via active power-frequency control and reactive power-voltage control loops, and adjust energy import(export) accordingly.

CRediT authorship contribution statement

A. Ahmad: Writing – review & editing, Writing – original draft, Project administration, Formal analysis. **J. Meyboom:** Visualization, Resources, Methodology, Formal analysis, Data curation. **P. Bauer:** Supervision, Resources, Project administration, Funding acquisition. **Z. Qin:** Writing – review & editing, Supervision, Methodology, Funding acquisition.

Declaration of competing interest

The authors declare that they have no known competing financial interests or personal relationships that could have appeared to influence the work reported in this paper.

Data availability

Data will be made available on request.

References

[1] NERC. Odessa disturbance report may-2021. 2021, [Online]. Available: https://www.nerc.com/pa/rrm/ea/Pages/May-June-2021-Odessa-Disturbance.aspx. [Accessed 11 October 2024].

[2] The Paris agreement, UNFCCC. 2015, [Online] Available: https://unfccc.int/sites/default/files/resource/parisagreement_publication.pdf. [Accessed 13 January 2024].

[3] CFP green buildings, grid congestion: what is it and how can you avoid it? 2023, [Online] Available: https://cfp.nl/en/news-and-cases/grid-congestion-what-is-it-and-how-can-you-avoid-it/. [Accessed 15 January 2024].

[4] Nicholas M, Hall D. Lessons learned on early fast electric vehicle charging systems. In: International council on clean transportation. Technical Report, Washington, DC, USA; 2018, [Online] Available: https://theicct.org/wp-content/uploads/2021/06/ZEV_fast_charging_white_paper_final.pdf. [Accessed 13 January 2024].

[5] IEA. Global EV outlook 2024. 2024, [Online]. Available: https://www.iea.org/reports/global-ev-outlook-2024. [Accessed 11 October 2024].

[6] Koolman G, Stecca M, Bauer P. Optimal battery energy storage system sizing for demand charge management in EV fast charging stations. In: Proc. IEEE transportation electrification conference & expo. ITEC, 2021, p. 588–94.

[7] Fastned, charging day presentation, fastned charging. 2022, [Online]. Available: https://www.fastnedcharging.com/media/lozn01dc/chargingdaypresentation-pdfversion3.pdf. [Accessed 11 October 2024].

[8] Fastned, everything you always wanted to know about fast charging. 2024, [Online] Available: https://fastnedcharging.com/hq/nl/why-fast-chargingstations-are-good-for-the-gridnl/. [Accessed 15 January 2024].

[9] Knupfer S, Noffsinger J, Sahdev S. How battery storage can help charge the electric-vehicle market, McKinsey & company. 2018, [Online]. Available: https://www.mckinsey.com/business-functions/sustainability/our-insights/how-battery-storage-can-help-charge-the-electric-vehicle-market. [Accessed 13 October 2024].

[10] He C, Zhang Y, Gong D, Ji X. A review of surrogate-assisted evolutionary algorithms for expensive optimization problems. Expert Syst Appl 2023;217:119495.

[11] Wu Y, Ravey A, Chrenko D, Miraoui A. A real time energy management for EV charging station integrated with local generations and energy storage system. In: Proc. IEEE transportation electrification conference and expo. ITEC, Long Beach, CA, USA; 2018, p. 1–6.

[12] Ahmad F, Ashraf I, Iqbal A, Khan I, Marzband M. Optimal location and energy management strategy for EV fast charging station with integration of renewable energy sources. In: Proc. IEEE silchar subsection conference. SILCON, Silchar, India; 2022, p. 1–6.

[13] Jia X, Li X, Quan H, Li Y, Dong L, Wu G. Cluster regulation architecture and control strategy of fast charging stations with energy storage system. In: Proc. IEEE 4th international conference on automation, electronics and electrical engineering. AUTEEE, Shenyang, China; 2021, p. 762–5.

[14] Cao Y, Wang N, Kamel G, Kim Y-J. An electric vehicle charging management scheme based on publish/subscribe communication framework. IEEE Syst J 2017;11(3):1822–35.

[15] Cao Y, Miao Y, Min G, Wang T, Zhao Z, Song H. Vehicular publish/subscribe (V-P/S) communication enabled on-the-move EV charging management. IEEE Commun Mag 2016;54(12):84–92.

[16] Ayyadi S, Ahsan SM, Khan HA, Arif SM. Optimized energy management system for cost-effective solar and storage integrated fast-charging station. In: 2024 IEEE power & energy society innovative smart grid technologies conference. ISGT, Washington, DC, USA; 2024, p. 1–5.

[17] Tan H, Chen D, Jing Z. Optimal sizing of energy storage system at fast charging stations under electricity market environment. In: 2019 IEEE 2nd international conference on power and energy applications. ICPEA, Singapore; 2019, p. 7–10.

[18] Liu G, Xue Y, Chinthavali MS, Tomsovic K. Optimal sizing of PV and energy storage in an electric vehicle extreme fast charging station. In: 2020 IEEE power & energy society innovative smart grid technologies conference. ISGT, Washington, DC, USA; 2020, p. 1–5.

[19] Liu J, Gao C, Cao Y. Multi-objective optimized configuration of electric vehicle fast charging station combined with PV generation and energy storage. In: Proc. IEEE 3rd international conference on electronics technology. ICET, Chengdu, China; 2020, p. 467–73.

[20] Smruthi Krishna K, Vijayasree G. Fast charging stations supported by flywheel energy storage systems. In: 2020 IEEE 5th international conference on computing communication and automation. ICCCA, Greater Noida, India; 2020, p. 109–13.

[21] Buchroithner others A. Grid load mitigation in EV fast charging stations through integration of a high-performance flywheel energy storage system with CFRP rotor. In: 2021 IEEE green energy and smart systems conference. IGESSC, Long Beach, CA, USA; 2021, p. 1–8.

[22] Ahmadi M, Kaleybar HJ, Brenna M, Castelli-Dezza F, Carmeli MS. DC railway micro grid adopting renewable energy and EV fast charging station. In: Proc. IEEE international conference on environment and electrical engineering and IEEE industrial and commercial power systems europe (EEEIC / i & CPS europe). Bari, Italy; 2021, p. 1–6.

[23] Schmidt O, Staffell I. Monetizing energy storage: a toolkit to assess future cost and value. Oxford University Press; 2024.

[24] de Rooij M. What are the different types of energy contracts in the netherlands? 2023, [Online] Available: https://www.keuze.nl/nieuws/wat-zijn-de-verschillende-soorten-energiecontracten-in-nederland#:~:text=Volgens%20cijfers%20van%20de%20Autoriteit,meest%20voorkomende%20energiecontract%20in%20Nederland. [Accessed 15 April 2024].

[25] StatLine. Natural gas and electricity, average end-user prices. 2023, [Online] Available:https://opendata.cbs.nl/statline/#/CBS/nl/dataset/81309NED/line?ts=1696241184616&fromstatweb=true. [Accessed 15 April 2024].

[26] TenneT. What kind of markets are there and how do they work? 2024, [Online] Available: https://netztransparenz.tennet.eu/electricity-market/about-the-electricity-market/what-kind-of-markets-are-there-and-how-do-they-work/. [Accessed 15 April 2024].

[27] Stedin. Wat betaalt uw bedrijf aan stedin? 2023, [Online] Available: https://www.stedin.net/zakelijk/betalingen-en-facturen/tarieven. [Accessed 15 January 2024].

[28] Mohammadi F, Saif M. A comprehensive overview of electric vehicle batteries market. E- Prime – Adv Electr Eng Electron Energy 2023;3:100127.

[29] Matworks. Why does energy density matter in batteries? 2024, [Online] Available: https://nl.mathworks.com/help/sps/powersys/ref/battery.html. [Accessed 15 January 2024].

[30] Stroe DI, Knap V, Swierczynski M, Stroe AI, Teodorescu R. Suggested operation of grid-connected lithium-ion battery energy storage system for primary frequency regulation: Lifetime perspective. In: Proc. IEEE energy conversion congress and exposition. ECCE, 2015, p. 1105–11.

[31] Andriunas I, Milojevic Z, Wade N, Das PK. Impact of solid-electrolyte interphase layer thickness on lithium-ion battery cell surface temperature. J Power Sources 2022;525:231126.

[32] Stroe DI, Knap V, Swierczynski M, Stroe AI, Teodorescu R. Operation of a grid-connected lithium-ion battery energy storage system for primary frequency regulation: A battery lifetime perspective. IEEE Trans Ind Appl 2017;53(1):430–8.

[33] Li K, Tseng KJ. Energy efficiency of lithium-ion battery used as energy storage devices in micro-grid. In: Proc. 41st annual conference of the IEEE industrial electronics society. 2015, p. 005235–40.

[34] Keil P, et al. Calendar aging of lithium-ion batteries. J Electrochem Soc 2016;163(9):8440.

[35] Tomaszewska A, et al. Lithium-ion battery fast charging: A review. ETransportation 2019;1:100011.

[36] Kumaravelu NK, D'Amico A, Rotonda M, Sinibaldi R, Orsini A, Falconi C. Burst noise in rechargeable LiFePO4 batteries and its changes after long-term calendar aging. J Power Sources 2023;581:233430.

[37] Najera J, et al. Semi-empirical ageing model for LFP and NMC li-ion battery chemistries. J Energy Storage 2016;72:108016.

[38] Wei J, Dong G, Chen Z. Remaining useful life prediction and state of health diagnosis for lithium-ion batteries using particle filter and support vector regression. IEEE Trans Ind Electron 2018;65(7):5634–43.

[39] Zhang S, et al. Synchronous estimation of state of health and remaining useful lifetime for lithium-ion battery using the incremental capacity and artificial neural networks. J Energy Storage 2019;26:100951.

[40] Ahmad A, Qin Z, Wijekoon T, Bauer P. An overview on medium voltage grid integration of ultra-fast charging stations: Current status and future trends. IEEE Open J Ind Electron Soc 2022;3:420–47.

[41] Electric vehicle conductive charging system—part 1: general requirements. Standard IEC 61851-1:2017, 2017, p. 1–287.

[42] Augustine S, Quiroz JE, Reno MJ, Brahma S. DC microgrid protection: review and challenges. Tech. Rep. SAND, Albuquerque, NM, USA: Sandia National Laboratories; 2018, p. 2018–8853.

[43] Yong JY, Ramachandaramurthy VK, Tan KM, Mithulananthan N. Bi-directional electric vehicle fast charging station with novel reactive power compensation for voltage regulation. Int J Electr Power Energy Syst 2015;64:300–10.

[44] Huber JE, Kolar JW. Volume/weight/cost comparison of a 1MVA 10kv/400v solid-state against a conventional low-frequency distribution transformer. In: Proc. IEEE energy conversion congress and exposition. ECCE, 2014, p. 4545–52.

[45] Shadfar H, Pashakolaei MG, Foroud AA. Solid-state transformers: An overview of the concept, topology, and its applications in the smart grid. Int Trans Electr Energy Syst 2021;31(9):12996.

[46] Mongird others K. Energy storage technology and cost characterization report. 2019, [Online]. Available: https://www.energy.gov/sites/default/files/2019/07/f65/Storage%20Cost%20and%20Performance%20Characterization%20Report_Final.pdf. [Accessed 11 March 2024].

[47] Gowda SN, Ahmadian A, Anantharaman V, Chu CC, Gadh R. Power management via integration of battery energy storage systems with electric bus charging. In: Proc. IEEE power energy society innovative smart grid technologies conf. ISGT, 2022, p. 1–5.

[48] Alibaba. 20 kw bidirectional DC/DC converter for energy storage system. 2024, [Online]. Available: https://www.alibaba.com/product-detail/20KW-bidirectional-DC-DC-converter-for_1600691943802.html. [Accessed 11 March 2024].

[49] Kim Y, Kim S. Forecasting charging demand of electric vehicles using time-series models. Energies 2021;14(5):1487.
[50] Uimonen S, Lehtonen M. Simulation of electric vehicle charging stations load profiles in office buildings based on occupancy data. Energies 2020;13(21):5700.
[51] Figenbaum E. Battery electric vehicle fast charging–evidence from the norwegian market. World Electr Veh J 2020;11(2):38.
[52] Hecht C, Figgener J, Sauer DU. Analysis of electric vehicle charging station usage and profitability in Germany based on empirical data. IScience 2022;25(12):105634.
[53] Fastned. Fastned hogenhoorn charging station. 2020, [Online]. Available: https://www.google.nl/maps/place/Fastned+Charging+Station/@52.0125328,4.3128451,700m/data=!3m1!1e3!4m6!3m5!1s0x47c5b43c1957f4a1:0xcccecfd9e0f79c16!8m2!3d52.0119373!4d4.3154809. [Accessed 11 October 2024].
[54] Fastned, fastned 2023 annual report. 2020, [Online]. Available: https://www.fastnedcharging.com/media/dysh0il1/fastned-2023-annual-report.pdf. [Accessed 11 October 2024].
[55] Fastned 2023, why fast charging stations are good for the grid? 2023, [Online]. Available: https://www.fastnedcharging.com/en/stories/why-fast-charging-stations-are-good-for-the-grid. [Accessed 15 April 2024].
[56] Santolaya ME, Casals LC, Corchero C. Estimation of electric vehicle battery capacity requirements based on synthetic cycles. Transp Res D: Transp Env 2023;114:103545.
[57] Huang Q, Mao J, Liu Y. An improved grid search algorithm of SVR parameters optimization. In: Proc. IEEE int. conf. commun. technol. 2012, p. 1022–6.
[58] Xing Z, Zhang Z, Guo J, Qin Y, Jia L. Rail train operation energy-saving optimization based on improved brute-force search. Appl Energy 2023;330(Part A):120345.
[59] Rocha T, Borges A, Paredes S, Pinho A. A matlab tool for solving linear goal programming problems. In: Proc. experiment int. conf. 2019, p. 337–42.
[60] Khond SV, Dhomane GA. Optimum coordination of directional overcurrent relays for combined overhead/cable distribution system with linear programming technique. Prot Control Mod Power Syst 2019;4(9).
[61] Sokoler LE, Frison G, Skajaa A, Halvgaard R, Jørgensen JB. A homogeneous and self-dual interior-point linear programming algorithm for economic model predictive control. IEEE Trans Autom Control 2016;61(8):2226–31.
[62] ENTSO-E transparency platform, day-ahead prices. 2023, [Online]. Available: https://transparency.entsoe.eu/. [Accessed 11 March 2024].
[63] Au H, et al. Beyond li-ion batteries: Performance, materials diversification, and sustainability. One Earth 2023;5(3):207–11.